Linkages between the North Pacific Oscillation and central tropical Pacific SSTs at low frequencies

Jason C. Furtado · Emanuele Di Lorenzo ·
Bruce T. Anderson · Niklas Schneider

Abstract The North Pacific Oscillation (NPO) recently (re-)emerged in the literature as a key atmospheric mode in Northern Hemisphere climate variability, especially in the Pacific sector. Defined as a dipole of sea level pressure (SLP) between, roughly, Alaska and Hawaii, the NPO is connected with downstream weather conditions over North America, serves as the atmospheric forcing pattern of the North Pacific Gyre Oscillation (NPGO), and is a potential mechanism linking extratropical atmospheric variability to El Niño events in the tropical Pacific. This paper explores further the forcing dynamics of the NPO and, in particular, that of its individual poles. Using observational data and experiments with a simple atmospheric general circulation model (AGCM), we illustrate that the southern pole of the NPO (i.e., the one near Hawaii) contains significant power at low frequencies (7–10 years), while the northern pole (i.e., the one near Alaska) has no dominant frequencies. When examining the low-frequency content of the NPO and its poles separately, we discover that low-frequency variations (periods >7 years) of the NPO (particularly its subtropical node) are intimately tied to variability in central equatorial Pacific sea surface temperatures (SSTs) associated with the El Niño-Modoki/Central Pacific Warming (CPW) phenomenon. This result suggests that fluctuations in subtropical North Pacific SLP are important to monitor for Pacific low-frequency climate change. Using the simple AGCM, we also illustrate that variability in central tropical Pacific SSTs drives a significant fraction of variability of the southern node of the NPO. Taken together, the results highlight important links between secondary modes (i.e., CPW-NPO-NPGO) in Pacific decadal variability, akin to already established relationships between the primary modes of Pacific climate variability (i.e., canonical El Niño, the Aleutian Low, and the Pacific Decadal Oscillation).

J. C. Furtado (✉) · E. Di Lorenzo
School of Earth and Atmospheric Sciences,
Georgia Institute of Technology, Atlanta, GA, USA
e-mail: jfurtado@aer.com

Present Address:
J. C. Furtado
Atmospheric and Environmental Research, Inc.,
131 Hartwell Ave., Lexington, MA 02421, USA

B. T. Anderson
Department of Geography and Environment,
Boston University, Boston, MA, USA

N. Schneider
International Pacific Research Center,
University of Hawaii at Manoa, Honolulu, HI, USA

1 Introduction

The prevailing paradigm of Pacific decadal climate variability centers around three prominent patterns in the Pacific atmosphere/ocean system: (1) the El Niño-Southern Oscillation (ENSO) phenomenon; (2) variability in the Aleutian Low (AL) induced by ENSO via the atmospheric bridge mechanism (e.g., Alexander et al. 2002); and (3) the Pacific Decadal Oscillation (PDO; Mantua et al. 1997), the latter of which can be thought of as the upper ocean of the North Pacific filtering the high frequency variability of the AL, thus reddening the response (e.g., Newman et al. 2003). Recently, impacts of climate change in the North Pacific and tropical Pacific have excited secondary modes
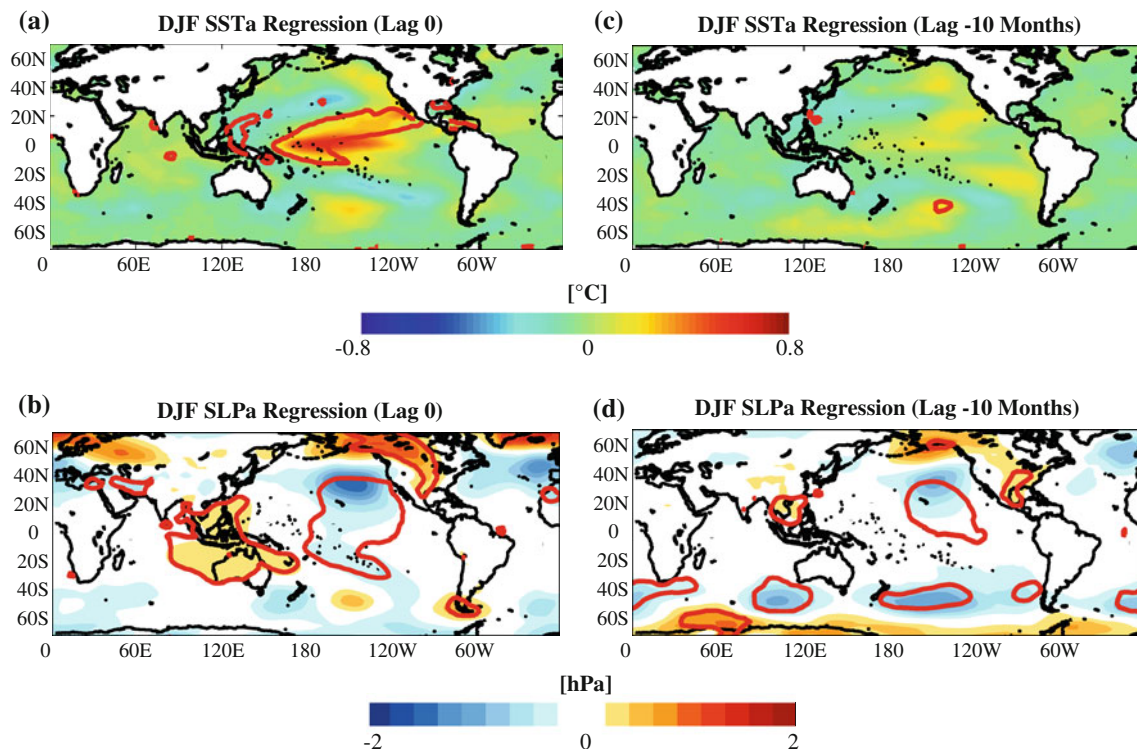
Fig. 1 a Regression of SSTa (°C) onto December–February (DJF) values of the standardized CPW index. **b** As in **a** but for SLPa (hPa). **c** As in **a** but for lag = −10 months. **d** As in **b** but for lag = −10 months. *Negative lag* indicates that the variable leads the CPW index. *Red contour* in all *plots* encloses areas where correlation coefficients are significant at the $p < 0.05$ level

of variability in the Pacific, providing potential new influences on Pacific decadal variability. One of these secondary modes involves a different "flavor" of ENSO known as "El Niño Modoki" (Ashok et al., 2007), or referred to in this paper as the Central Pacific Warming (CPW) phenomenon. Formally defined as the second leading pattern of variability of tropical Pacific sea surface temperature (SST), the CPW phenomenon exhibits maximum positive SST anomalies (SSTa) in the central tropical Pacific, rather than the eastern tropical Pacific as seen during "traditional" or "canonical" ENSO episodes, with negative SSTa to the east and west of the positive SSTa (see Fig. 1a). The different tropical Pacific SSTa pattern also yields a unique extratropical atmospheric response compared to that found during a canonical ENSO event.

Unlike the projection of ENSO on the AL, CPW variability projects on a very different sea level pressure (SLP) pattern in the North Pacific. Figure 1b illustrates that the North Pacific SLP anomaly (SLPa) pattern associated with the CPW phenomenon is a north-south dipole in pressure between northwestern North America and just north of Hawaii. This pattern is closely related to the North Pacific Oscillation (NPO), the second leading mode of North Pacific SLPa (Walker and Bliss 1932; Rogers 1981; Linkin and Nigam 2008). The NPO has also been linked as a precursor signature to positive ENSO/CPW events (e.g.,

Vimont et al. 2001, 2003; Anderson 2003, 2007a; Ashok et al. 2007) particularly the node near Hawaii (Anderson 2003 2007a; Ashok et al. 2007). Indeed, while the CPW SSTa signature is weak during the previous boreal spring (Fig. 1c), an NPO-like signature is still visible in the North Pacific, with largest anomalies in the southern node (Fig. 1d).[1] Given that CPW activity is forecasted to increase in frequency and magnitude under future climate change (Yeh et al. 2009), understanding the associated changes in the extratropical response, and hence better understanding the NPO warrants more attention.

Previous studies on the NPO have centered on two main topics. One topic is the role of the NPO in the initiation and development of the ENSO system by modifying the wind-stress fields over the North Pacific, which in turn produce a boreal spring basin-scale SST structure that is optimal for ENSO growth the following winter (e.g., Penland and Sardeshmukh 1995). This SST "footprint" can also persist into the summer when it can subsequently force the overlying atmosphere, resulting in zonal wind stress anomalies that are conducive to initiating an ENSO event (the

---

[1] We also note that Fig. 1d shows a somewhat zonally-symmetric negative SLP anomaly in the mid-latitudes of the Southern Hemisphere. Since the signal is not persistent at the height of a CPW event (Fig. 1b) and our focus is on North Pacific decadal variability, we leave this finding as an observation only.

"Seasonal Footprinting Mechanism"; Vimont et al. 2001 2003). Alternatively, the NPO-induced wind stress anomalies may produce concurrent subsurface temperature and heat content anomalies in the central and eastern tropical Pacific that can influence central and eastern equatorial Pacific SSTa through the rest of the year (Anderson 2004, 2007b; Anderson and Maloney 2006). The second topic of interest with the NPO is the associated teleconnection patterns impacting North American wintertime weather and climate (e.g., Rogers 1981; Linkin and Nigam 2008). For example, the positive phase of the NPO promotes drier conditions along northwestern North America and increased chances for cold air outbreaks in the central and eastern United States (e.g., Walker and Bliss 1932; Rogers 1981; Linkin and Nigam 2008). Though different in scope, these two topics have focused on the NPO on short (weekly to seasonal) timescales but did not examine the potential role the NPO plays in long-term (e.g., decadal) climate.

This study diagnoses further the dynamics of the NPO with a focus on decadal-scale variability. As the NPO itself is a stochastic mode of variability (e.g., Rogers 1981), we will first show that a portion of the NPO (its southern node) contains significant low-frequency variability. The northern node of the NPO is white in frequency content, as is the NPO itself. Therefore, the impact of the NPO on seasonal, interannual and decadal climate variability depends on whether a node or the entire oscillation is considered. From there, we will illustrate that the low-frequency nature of the NPO southern node is dynamically tied to CPW-type variability, much as it is at seasonal timescales (e.g., Di Lorenzo et al. 2010).

Section 2 presents an overview of the data, the model experiments, and statistical methods employed. Statistical links between the NPO and the CPW are presented in Sect. 3. A detailed examination of the NPO and its individual poles in observations is presented in Sect. 4. Section 5 then decomposes the NPO and its poles into their low-frequency component to illustrate the explanatory power of each pole separately at quasi-decadal scales. A mechanism for the connections between the CPW and the extratropical North Pacific atmospheric circulation is then proposed in Sect. 6. Discussion of the results and implications for future studies on North Pacific climate variability follow.

2 Data and methods

2.1 Observational data

Atmospheric variables used in the study originate from the National Center for Environmental Prediction/National Center for Atmospheric Research (NCEP/NCAR) Reanalysis Project (Kistler et al. 2001). The data reside on a 2.5°

by 2.5° horizontal grid and 17 vertical pressure levels, ranging non-uniformly from 1000 to 10 hPa. We use primarily SLP data throughout the study, but in Sect. 6, we analyze streamfunction at 200 hPa to connect CPW-type variability and the atmospheric circulation of the North Pacific. Monthly-mean values of the variables from 1950 to 2008 are analyzed with a focus on boreal winter values (November–March; NDJFM).

The only observed oceanic variable used in our analysis is SST from the National Oceanic and Atmospheric Administration Extended Reconstruction SST dataset (NOAA ER SSTs), version 3 (Smith et al. 2008). The monthly-mean SST values from the NOAA ER SSTs are gridded on a 2° by 2° horizontal grid globally. The data used in the analyses span 1950–2008 and are monthly-mean values.

Anomalies are defined as the departure from the 1950 to 2008 climatological values for each month. All data are linearly detrended before statistics are computed.

2.2 ICTP model experiments

Model experiments for testing the influence of tropical Pacific SST variability on the NPO are done using the International Centre for Theoretical Physics (ICTP) atmospheric general circulation model (AGCM), also known as "SPEEDY" (Simplified Parameterization, primitivE-Equation DYnamics). The model atmosphere consists of eight vertical layers and T30 horizontal resolution (3.75° by 3.75° on a longitude/latitude grid). The physical parameterizations of the model are described in Molteni (2003), and prior applications of the model in various configurations can be found in Bracco et al. (2006), Kucharski et al. (2006, 2007).

Two experiments are run with the ICTP AGCM. One experiment consists of the model forced by prescribed time-varying SSTa globally from 1950–2008 (herein referred to as the CONTROL run). This run depicts how well the model performs in recreating the various relationships associated with the NPO and SSTa. The second integration of the model is the same that was used by Di Lorenzo et al. (2010). The run uses prescribed time-varying SSTa over the equatorial Pacific Ocean (12°S–12°N) only, while elsewhere an interactive mixed layer model is used with constant depth of 50 m. For the mixed layer configuration, a heat flux climatology is generated from a previous integration of the model that is forced with the NOAA ER SSTs from 1950 to 2008. This experiment, which consists of 45 ensemble members, is referred to as the TROP run. Each ensemble member differs by randomizing the tropical Pacific SSTa forcing for the first 2 years of the integration, and then allowing the model atmosphere to evolve thereafter. Hence, for both the CONTROL and TROP runs, we only use output from

1953 to 2008 for analysis to exclude the "spin-up" time. Statistics and results shown from the TROP runs are derived from the ensemble-mean statistics (i.e., statistics are computed for each ensemble member separately and then averaged together). This method of ensemble averaging allows us to retain both the signal from the tropical SSTa forcing and also some of the "noise" from each ensemble member.

2.3 Index definitions

2.3.1 The NPO index

The NPO is generally defined as the second leading empirical orthogonal function (EOF-2) of NDJFM North Pacific SLPa poleward of 15° N (e.g., Vimont et al. 2003). However, using an EOF-based definition for the AGCM runs is not ideal because EOF patterns of model variables may not match spatially nor in rank with those of observations. Instead, we define the NPO using a different approach. First, using observations, we compute EOF-2 of NDJFM North Pacific SLPa and produce a correlation map between NDJFM SLPa and the second principal component (PC) time series. The two loading centers of the NPO are identified and used to define two additional indices: the NPO NorthPole (NPO NP) and NPO SouthPole (NPO SP) indices; i.e., the area-averaged monthly-mean SLPa within the nodes. The NPO index is defined then simply as:

$$NPO(t) = NPO_{NP}(t) - NPO_{SP}(t) \qquad (1)$$

Figure 2a illustrates the observed NPO signature obtained from this procedure, along with gray boxes denoting the regions where the NPO NP and NPO SP are defined (see caption of Fig. 2 for definitions of the boundaries). The characteristic dipole of the NPO is clearly recovered using this method. Furthermore, the correlation between the NPO index computed using (1) and that from EOF analysis (i.e., the expansion coefficient time series from projecting monthly SLPa maps onto EOF-2) is $r = 0.98$, further validating this approach. Figure 2b and c show the NPO signature in the model runs. The model NPO index and indices of its individual poles are computed as done for observations—that is, SLPa are area-averaged over the two same two gray boxes depicted in Fig. 2a but in the model domain, and then the two are subtracted to form the NPO index. The spatial correlations for the model maps compared to the observations are $r = 0.91$ for the ICTP CONTROL run and $r = 0.87$ for the ensemble-mean ICTP TROP runs.

2.3.2 The CPW index

In this study, the CPW index is defined as the second PC time series of monthly-mean tropical Pacific SSTa

(a) SLPa Correlated with NPO Index (OBS)

(b) SLPa Correlated with NPO Index (CONTROL)

(c) SLPa Correlated with NPO Index (TROP ENSMEAN PATTERN)
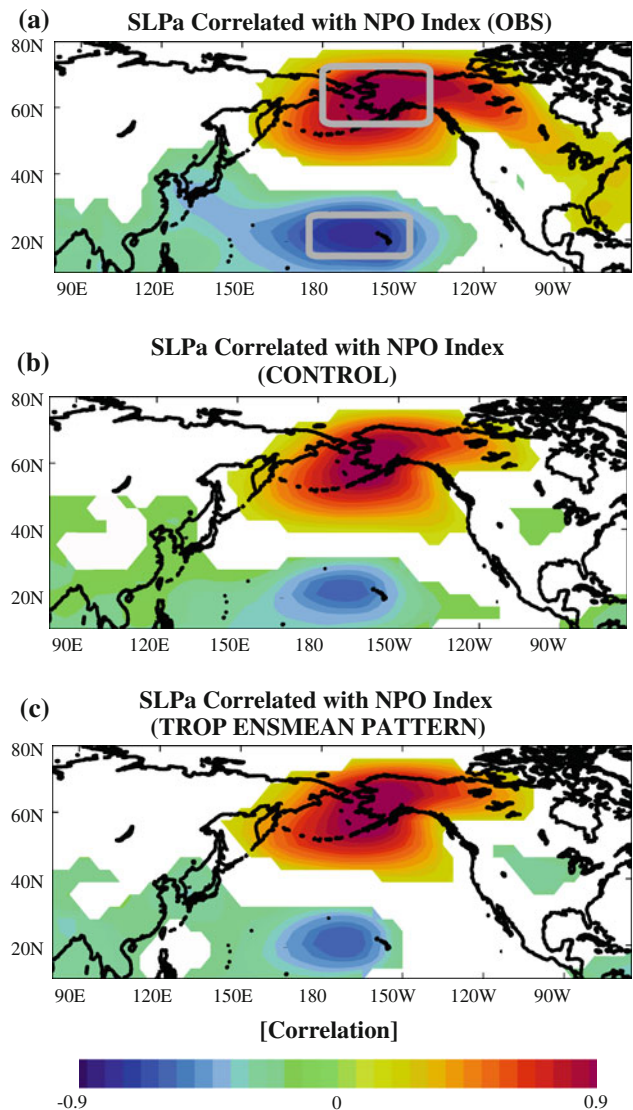
[Correlation]

-0.9 0 0.9

Fig. 2 a Correlation of observed NDJFM SLPa with the standardized NPO index from observations. *Gray boxes* denote the locations of the area-averaged SLPa used to compute the NPO NorthPole (northernmost box; 55°–72.5°N; 180°–140°W) and NPO SouthPole (southernmost box; 15°–27.5°N; 175°E–147.5°W). **b** As in **a** but for SLPa and NPO index from the output of the CONTROL run. **c** As in **a** but the ensemble-mean SLPa correlation pattern of the TROP runs. In all *plots*, only correlations exceeding the 99% significance level are plotted

(20° S–20° N, 80° E - 60° W), similar to the definition used by Ashok et al. (2007). This PC time series explains nearly 10% of the variance in tropical Pacific SSTa from 1950 to 2008. Indeed, as the frequency of CPW events have increased over the last 20–30 years, the percent variance of tropical Pacific SSTa variability explained by the CPW mode has increased (up to just above 12% when only the last 20 years of SSTs are used, as in Ashok et al. (2007)). Using PC-2 of tropical Pacific SSTa is similar to using the El Niño-Modoki Index as defined by Ashok et al.

(2007) (which is derived from the loading centers of EOF-2 of tropical Pacific SSTs), with the two indices correlated at $r = 0.87$ ($p < 0.01$).

2.4 Statistical methods

Power spectrum analysis and filtering are the two primary techniques in isolating variability at different frequencies for the NPO. The NPO power spectra are calculated using year-round, monthly-mean values of the indices and are normalized so that values represent the percent of variance explained at a particular period, with the total area under the curve equal to 100%. Time series are subdivided three times, and a three-point running mean is applied to the power spectra, increasing the degrees of freedom for the power spectrum analysis ninefold. Peaks that are referred to as "significant" in the text are those peaks which pass the F-statistic test at the 95% significance level, as described by Torrence and Compo (1998). For filtering of the time series, the Fourier transform method is used. Since this method is problematic at the ends of time series, the first and last year of the time series (i.e., 12 values on either side) are discarded post-filtering when calculating correlations with the filtered time series.

Relationships between the NPO and other atmospheric and oceanic variables are deduced through linear regression and correlation analysis. The significance of correlation coefficients is determined in two ways (both of which are complementary and yield very similar significance): using a two-tailed Student-t test and through a bootstrap approach. Significance testing for the correlations using the t-statistic relies on identifying the number of independent samples in the analysis. To account for autocorrelation in the indices and fields used in the correlation analyses, we follow the definition of the effective degrees of freedom N_{eff} defined in Bretherton et al. (1999):

$$N_{\text{eff}} = N \frac{1 - r_1 r_2}{1 + r_1 r_2} \tag{2}$$

where N is the total sample size and r_1 and r_2 are the lag-1 autocorrelations of the index and field being correlated, respectively.

For the bootstrap approach, the original time series are decomposed into their Fourier series, and subsequently 2000 red-noise time series with the same lag-1 correlation coefficient are simulated. However, for each red-noise time series, the phases of the original time series are randomized. The probability density function (PDF) of the cross-correlation between those simulated series is then computed. Desired significance levels (e.g., the 95% and 99% significance levels) are found by computing the area under the PDF and comparing those values to the cross-correlation

between the two time series in question to accept or reject the null hypothesis (i.e., $r = 0$).

3 Establishing the NPO-CPW relationship in observations

Figure 3 presents the characteristics of the CPW index in time and contrasts it with the canonical ENSO signature, here represented by the leading PC of tropical Pacific SST variability. The monthly standardized CPW time series (Fig. 3a; black line) displays variability at multiple frequencies. Year-to-year variations are evident as is a low-frequency envelope of variability in the index, with a tendency toward more low frequency variability toward modern times. By contrast, PC-1 of tropical Pacific SST variability (hereafter referred to as the CanENSO index; Fig. 3a; gray line) shows relatively regular variance throughout the record, though punctuated with extremely positive events in 1972–1973, 1982–1983, and 1997–1998. Except for the 1972–1973 event, the latter two positive canonical ENSO events featured strongly negative values of the CPW index, indicating that the maximum warming for those events were in the eastern equatorial Pacific. Also note that during the early- and mid-1990s, positive values of the CPW index dominate the record, consistent with the prolonged El Niño state of the tropical
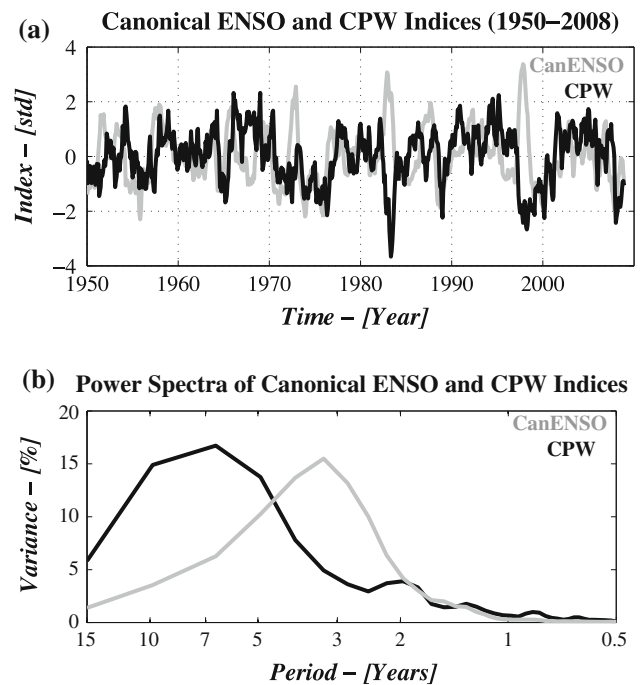
Fig. 3 **a** Monthly standardized CPW index (*black*) and the CanENSO index (i.e., PC-1 of tropical Pacific SST variability; *gray*) from 1950 to 2008. **b** Power spectrum (plotted as percent variance) as a function of period (years) of the CPW index (*solid black*) and the CanENSO index (*solid gray*) from 1950 to 2008

Pacific observed at that time (e.g., Goddard and Graham 1997; van Loon et al. 2003).

The spectral behavior of the CPW phenomenon also exhibits differences from the CanENSO index (Fig. 3b). The power spectrum of the CanENSO index (Fig. 3b; gray line) displays the established interannual peak of the ENSO phenomenon between 2 and 5 years. By contrast, the power spectrum of the CPW index has two different peaks: one at biannual periods and a stronger, much broader peak between 5 and 13 years (Fig. 3b; black line). To test the robustness of the peaks in the CPW power spectrum, the CPW index was recalculated from 1870 to 2008 using both the NOAA ER SSTs and also the Hadley Centre Sea Ice and Sea Surface Temperature (HadISST) dataset (Rayner et al. 2003). Power spectrum analysis of those two longer time series (and 58-year long subsets) recovered the same two peaks in the CPW index. Thus, we confidently conclude that, unlike eastern Pacific warmings, the CPW phenomenon exhibits a pronounced signal at the quasi-decadal timescale, implying that this type of El Niño may play a unique role in Pacific decadal climate variability different from the canonical ENSO influence.

Connections between the CPW phenomenon and climate variability in the North Pacific are summarized in Fig. 4. The correlation between SLPa and the CPW index

(Fig. 4a) illustrates that warmings of the central equatorial Pacific are associated with a broad region of negative SLPa throughout the subtropical North Pacific, extending into the central tropical Pacific and even portions of the subtropical South Pacific. Significant correlations ($p < 0.05$; outlined by the thick red line in all panels of Fig. 4) also exist in the far eastern tropical Pacific and across central North America and Alaska. The extratropical North Pacific SLPa signature has strong similarities to the characteristic NPO signature (see Fig. 2a). The SSTa correlation map (Fig. 4b) shows the strongest correlations to be throughout the central equatorial Pacific, extending northeastward toward Hawaii and Baja California.

To highlight connections between the NPO and the CPW at quasi-decadal scales, Fig. 4c and d display the correlations between SLPa (Fig. 4c) and SSTa (Fig. 4d) with the low-pass filtered (periods >7 years retained) NPO index. The choice of 7 years and longer for the low-pass filter was made based on the peak in the power spectrum of the CPW index and to avoid the interannual variability from the canonical ENSO phenomenon (Fig. 3b). The SLPa correlation plot illustrates that at low frequencies, the NPO is still evident, though highest correlations exist in the subtropical North Pacific near Hawaii. This area of anti-correlation coincides with the anti-correlation center in
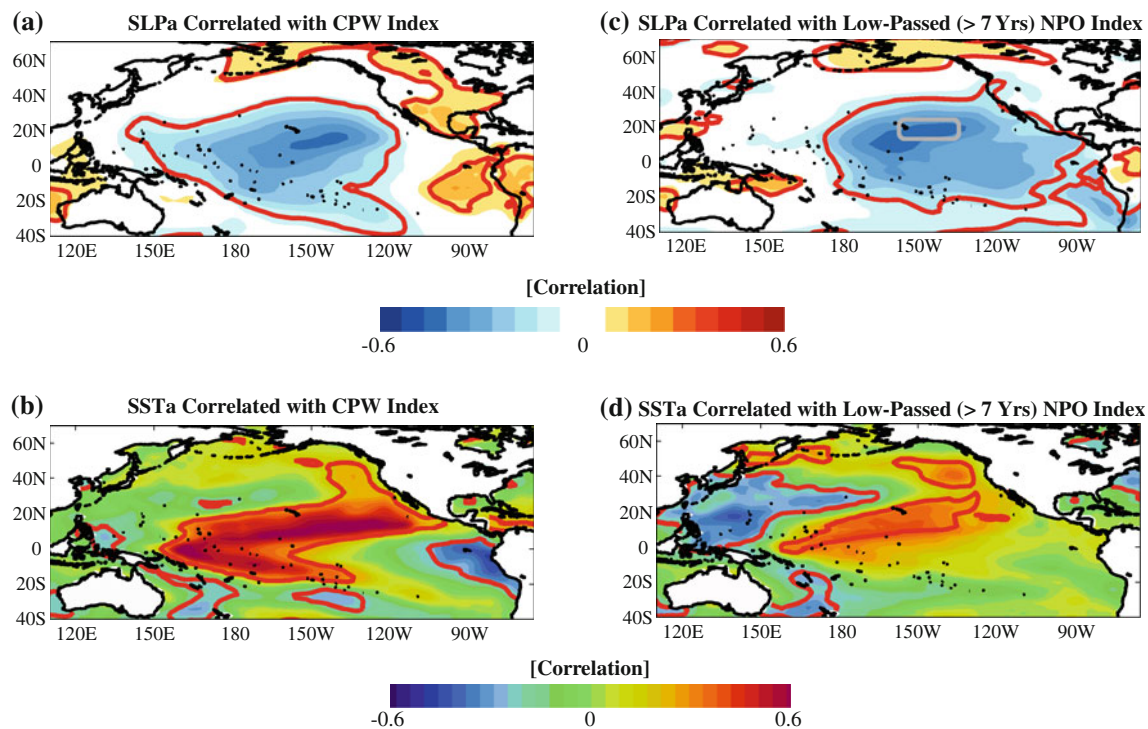

Fig. 4 **a** Correlation of observed monthly-mean SLPa with the standardized CPW index. **b** As in **a** but for monthly-mean SSTa. **c** As in **a** but for the observed low-passed (periods > 7 years retained) monthly-mean NPO index. **d** As in **b** but for the observed low-passed monthly-mean NPO index. *Red contour* in all *plots* encloses correlation coefficients that exceed the $p < 0.05$ level. *Gray box* in **c** outlines the boundary for the SLPa Hawaii index (see *text*)

the CPW correlation map (Fig. 4a). Moreover, the SSTa correlation map with the low-passed NPO index (Fig. 4d) shows a pattern very similar to the CPW (Fig. 4b), but also with significant negative correlations in the far western Pacific. Such similarities between the CPW correlation maps and the low-passed NPO maps indicate that the CPW may contribute to low-frequency variability in the subtropical North Pacific atmosphere in addition to the North Pacific Ocean (e.g., Di Lorenzo et al. 2010).

4 Analysis of the NPO and its individual poles

Section 3 established a clear link in the ocean and atmosphere between variability in the CPW and NPO, both at seasonal timescales and quasi-decadal timescales. In particular, the CPW shares a common area of variance with the low-passed NPO in the subtropical North Pacific near Hawaii. Thus, while the NPO by its original definition denotes a see-saw in SLP between Alaska and Hawaii, its poles individually may play different roles in Pacific climate variability.

Table 1 shows the correlations between four indices used to measure variability in the NPO: the NPO index from (1), the NPO NP, the NPO SP, and an index of the average SLPa near Hawaii (called the SLPa Hawaii index), in observations and the two model runs. The SLPa Hawaii index is defined as in Di Lorenzo et al. (2010) (i.e., the area-averaged SLPa between 158°W–135°W, 13°N–24°N) and is included for two reasons. One is its use in previous studies concerning ENSO precursor/CPW activity (e.g., Anderson 2003, 2007a). Secondly, this index overlaps the broad region of subtropical North Pacific SLPa that is correlated with the low-passed NPO index (gray box in Fig. 4c denotes the boundaries for the SLPa Hawaii index), and as such, is representative of the low-frequency signature of the NPO SP.

For the observations, the NPO index is nearly identical to the NPO NP index (correlation close to unity; Table 1). This high correlation suggests that the NPO index is overwhelmingly dominated by the variability in its northern node. The weakest correlations seen in observations are between the NPO NP and the NPO SP ($r = -0.59$) and the SLPa Hawaii ($r = -0.37$) indices. The correlation coefficients for the CONTROL run match very well with the observations, except the relationships between the NPO/NPO SP and NPO NP/NPO SP are weaker. However, the model has virtually no relationship between its NPO NP and SLPa Hawaii indices ($r = -0.08$). For the TROP runs, all correlations are nearly identical to those in the CONTROL run, though the NPO/NPO SP correlation increases slightly ($r = -0.44$ for the CONTROL; $r = -0.50$ for the TROP ensemble-mean). Overall, the results in Table 1 indicate that (a) the NPO index is strongly tied to the NPO NP variability more than its southern node, even in the AGCM, and (b) the NPO NP and the subtropical North Pacific SLPa (represented by either the NPO SP or SLPa Hawaii) indices are among the least related, particularly in the model between the NPO NP and SLPa Hawaii indices.

Figure 5a presents the power spectra of the NPO index (black curve), the NPO NP index (red curve), the NPO SP index (blue curve), and the SLPa Hawaii index (gray curve) from observations. For the NPO index, the power spectrum is relatively flat, with minor peaks at periods <1 year and a slight increase in power in the 3–6 year band. The power spectrum of the NPO NP index (Fig. 5a, red curve) follows closely that of the NPO index, with a local maximum in the 2–3 year band and decreasing power thereafter. None of the peaks for the NPO or NPO NP power spectrum at periods larger than 1 year are significant at the $p < 0.05$ level. The NPO SP power spectrum, by contrast, has a significant peak in the 4–9 year band (dashed blue line in Fig. 5a represents the 95% significance level). Finally, the SLPa Hawaii index (Fig. 5a; gray line) exhibits significant power at periods of ~3–15 years. The enhancement of decadal-scale power for the SLPa Hawaii over the NPO SP follows from earlier results illustrated in Figs. 2a and 4c. At higher frequencies, the NPO takes on its characteristic meridional dipole structure (Fig. 2a), but at low frequencies the

Table 1 The cross-correlation between the monthly-mean four indices used to describe NPO variability for observations, the CONTROL run, and the TROP runs (i.e., the ensemble-mean correlation)

Correlated Indices	Observations	CONTROL	TROP ENSMEAN
r(NPO, NPO NP)	0.97**	0.97**	0.97**
r(NPO, NPO SP)	−0.74**	−0.44**	−0.50**
r(NPO, SLPa Hawaii)	−0.50**	−0.27**	−0.26**
r(NPO NP, NPO SP)	−0.59**	−0.22**	−0.25**
r(NPO NP, SLPa Hawaii)	−0.37**	−0.08	−0.05
r(NPO SP, SLPa Hawaii)	0.76**	0.83**	0.80**

Correlations with a double asterisk (**) are significant at the $p < 0.01$ level
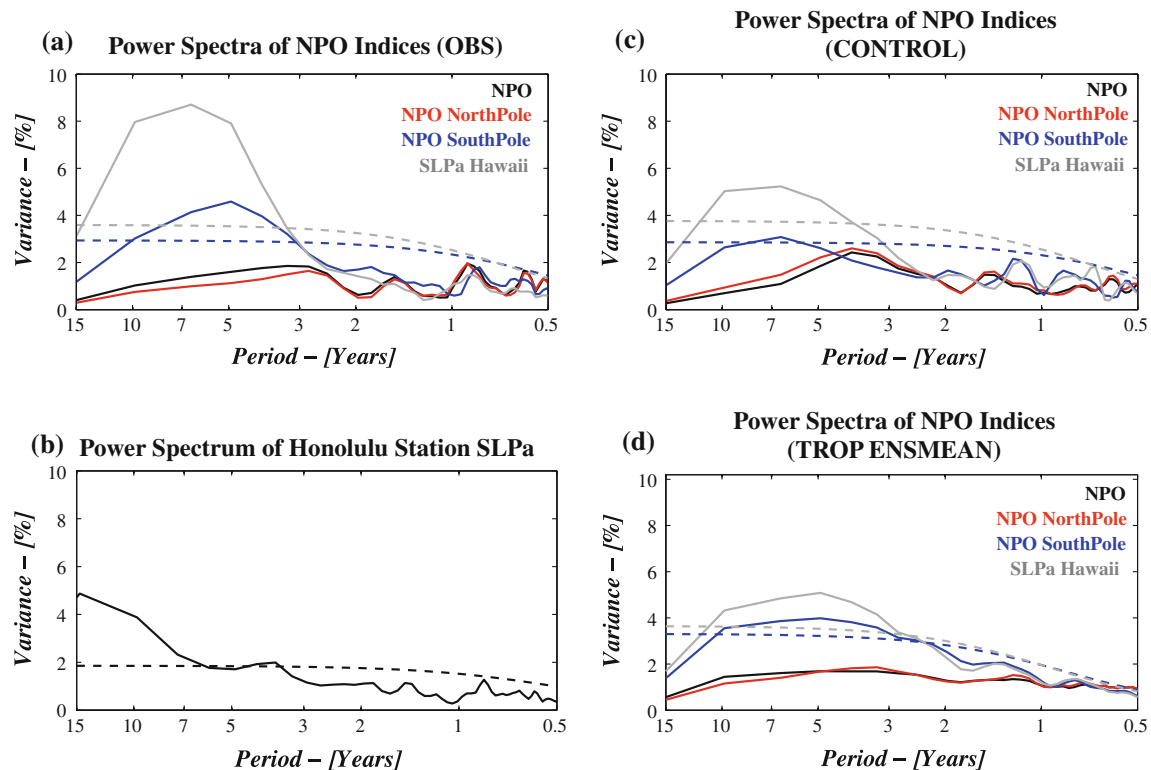
Fig. 5 a Power spectra (plotted as percent variance) of the NPO index (*solid black*), the NPO NP index (*solid red*), the NPO SP index (*solid blue*), and the SLPa Hawaii index (*solid gray*). *Dashed blue* (*gray*) *line* denotes the 95% significance curve for the NPO SP (SLPa Hawaii) power spectrum. **b** Power spectrum (*solid black*) of a station record of Honolulu SLP from 1921 to 2008. *Dashed black line* denotes 95% significance curve. **c** As in **a** but for the ICTP CONTROL run. **d** As in **a** but for the ensemble-mean spectra of the indices from the ICTP TROP runs

subtropical node of the NPO shifts eastward and is now best represented by our SLPa Hawaii index (Fig. 4c).

Hence, the existence of interannual and decadal-scale power in/near the subtropical node of the NPO indicates that the NPO phenomenon may not be wholly stochastic as previous studies suggested. Moreover, the similarity in the power spectra of the SLPa Hawaii index and the CPW index (Fig. 3b) further implies a dynamical connection between the two. To test the robustness of the SLPa Hawaii spectrum, power spectrum analysis is repeated for a station record of monthly-mean SLPa from Honolulu, HI, from 1921 to 2008 (Fig. 5b; Quayle 1989).[2] Indeed, the Honolulu station record does exhibit enhanced significant power at low frequencies (7–15 years and beyond).

The power spectra for the NPO indices from the ICTP model runs are shown in Fig. 5c (CONTROL) and d (TROP ENSMEAN). In the CONTROL run (Fig. 5c), the spectra follow the observations well in structure, though the magnitude of power for the NPO SP and SLPa Hawaii

---

[2] The data were downloaded from the Data Support Section (DSS) of the Computational and Information Systems Laboratory (CISL) at NCAR—http://dss.ucar.edu/datasets/ds570.0/.

indices is less than their observational counterparts at quasi-decadal scales. The SLPa Hawaii index still retains significance in the ∼4–13 year band, but the NPO SP power spectrum loses almost all of its significance, with a single peak just passing significance at the ∼7 year period. The reductions in overall power and significance of the NPO SP power spectrum (as well as the reduction of power of the SLPa Hawaii spectrum) are consistent with the damping of low-frequency atmospheric signals in AGCMs forced with prescribed time-varying mid-latitude SSTs (e.g., Bladé 1997; Barsugli and Battisti 1998).

The ensemble-mean power spectra from the ICTP TROP runs recover much of the characteristics of the observed spectra, including at low frequencies (Fig. 5d). The power spectra of the NPO and NPO NP indices remain relatively flat for all periods, including high frequencies. However, the SLPa Hawaii and NPO SP power spectra in the ensemble-mean display interannual to decadal scale variability, with broader peaks for both indices compared to the observed and the CONTROL (Fig. 5a and c) spectra. Most of the low-frequency signature of the NPO SP and SLPa Hawaii spectra are now significant compared to the CONTROL run results. Overall, the ensemble-mean results indicate that the tropical Pacific SSTa forcing alone

enhances power to the low-frequency content of the subtropical North Pacific SLP indices.

5 Low-Frequency NPO signatures in Pacific SSTs

5.1 Observations

Based on analyses already presented and the work done by Di Lorenzo et al. (2010), we hypothesize that low-frequency changes in the NPO, particularly in the NPO SP, are directly related to CPW-type variability in the tropical Pacific SSTa field. SSTa correlation maps with the low-passed NPO indices (periods >7 years retained) indeed illustrate strong connections between North Pacific SLPa variability and the CPW phenomenon (Fig. 6). Using the low-passed NPO SP and SLPa Hawaii indices (Fig. 6c and d) produce very similar SSTa correlation maps to that of the CPW (Fig. 4b) with strong positive correlations extending from the far western tropical Pacific Ocean northeastward just south of Hawaii and up the North American coast flanked by negative correlations. Much of the signal in the subtropical Pacific and parts of the central tropical Pacific is significant at the $p < 0.05$ level in both plots (gray contours in Fig. 6c and d). For the SSTa correlation map associated with the low-passed NPO index (Fig. 6a), the signal across the far northern and northwestern Pacific Ocean is stronger than in the NPO SP or SLPa Hawaii correlation maps, while the positive correlations in the subtropical and tropical Pacific Ocean are lower in magnitude. The SSTa correlation map with the low-passed NPO NP index, however, has a slightly different pattern (Fig. 6b). Maximum positive correlations exist in the far North Pacific, rather than the subtropical North Pacific and tropical Pacific. This region of maximum correlation matches where the correlation between SSTa and the low-passed NPO index has a local maximum (Fig. 6a). This result is expected—recall from Table 1 that the NPO and NPO NP index are virtually identical, as are their power spectra (Fig. 5a).

More evidence of the dominance of the NPO SP and SLPa Hawaii in low-frequency connections with the tropical Pacific SSTa and the CPW phenomenon is shown in Fig. 7. When correlating the low-passed versions of the CPW index with the low-passed NPO or NPO NP indices, the correlations are insignificant ($r = 0.56$ and $r = 0.31$, respectively). However, for the NPO SP and SLPa Hawaii indices, the correlations are high and significant ($r = 0.77$; $p < 0.05$; Fig. 7c and d). In particular, for most of the 1990s, a time of moderate CPW activity (Fig. 3a; black line), the low-passed NPO SP and SLPa Hawaii indices almost perfectly coincide with the low-passed CPW index.
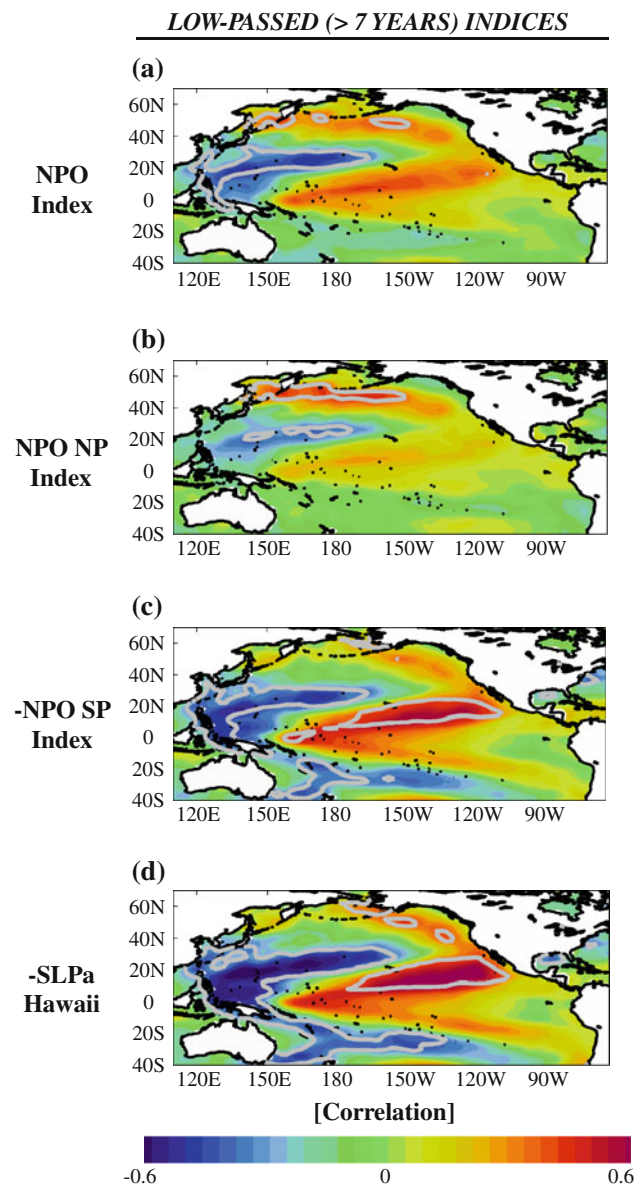
LOW-PASSED (> 7 YEARS) INDICES

Fig. 6 Correlation of observed NDJFM SSTa with the standardized low-passed NPO indices for observations: **a** NPO index; **b** NPO NP index; **c** NPO SP index (*inverted*); (**d**) SLPa Hawaii index (*inverted*). *Gray contour* in all *plots* outlines where correlations are significant at the $p < 0.05$ level

5.2 ICTP model results

We now use the ICTP TROP runs to test our hypothesis that tropical Pacific SSTa variability forces and drives low-frequency NPO SP variations. Di Lorenzo et al. (2010) have shown that subtropical North Pacific SLPa, particularly in the Hawaiian region, share variance with central tropical Pacific SSTa variability, which is then integrated into the signature of the NPGO in the North Pacific. Whether the model also captures the low-frequency connections between the NPO SP and tropical Pacific SSTa
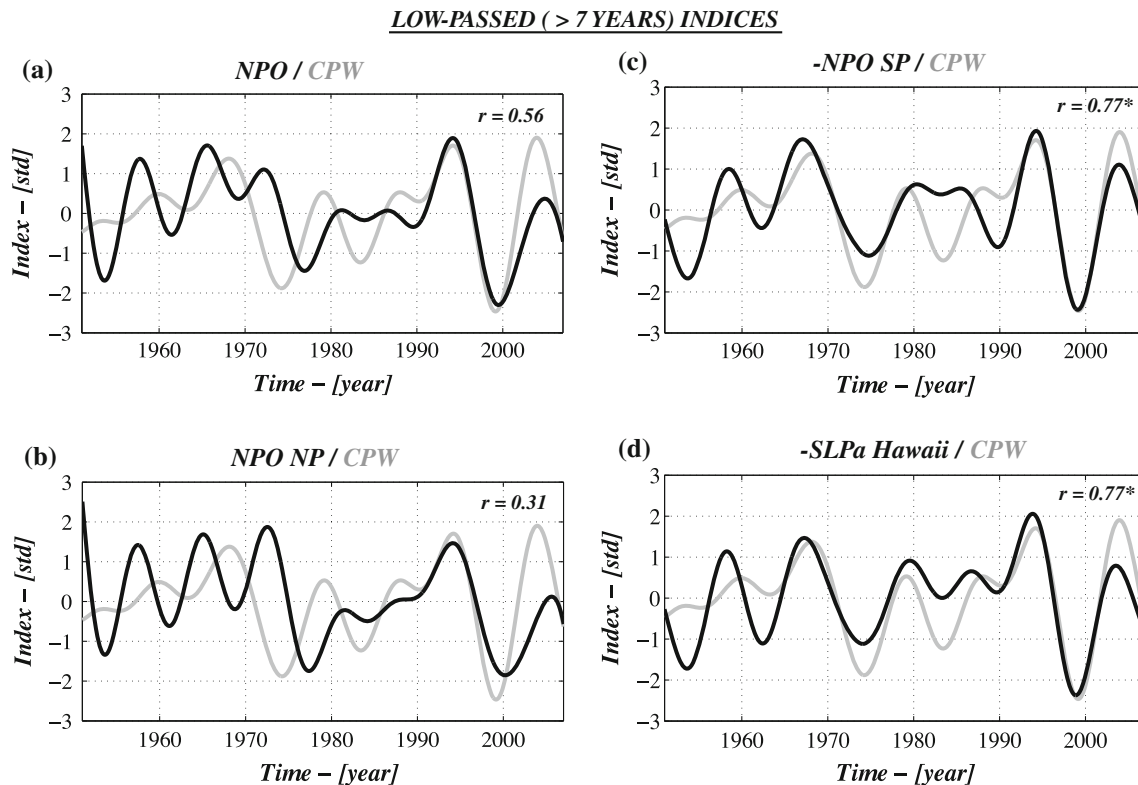
LOW-PASSED (> 7 YEARS) INDICES

Fig. 7 a The observed standardized low-passed NPO index (*black*) and low-passed CPW index (*gray*) from 1951 to 2007. **b** As in **a** but with the standardized low-passed NPO NP index (*black*). **c** As in **a** but with the standardized low-passed NPO SP index (*inverted; black*).

d As in **a** but with the standardized low-passed SLPa Hawaii index (*inverted; black*). Correlations between the two indices indicated in each *panel*. Single asterisk (*) denotes that the correlation is significant at the $p < 0.05$ level

variability is tested here. Figure 8 shows the CONTROL and TROP ENSMEAN correlation maps between the tropical Pacific SSTa in the model and the low-passed versions of the four NPO indices. In Fig. 8, model results are restricted to the equatorial Pacific as this is the common region of prescribed, observed SSTs in both runs. Immediately noticeable is the difference between using the low-passed NPO/NPO NP and NPO SP/SLPa Hawaii indices in the correlations. The CONTROL and TROP ENSMEAN NPO/NPO NP correlation plots (Fig. 8a, b and e, f) show that these indices have almost no correlation or even weak *negative* correlations with SSTa in the tropics, contrary to what we see in the observations (Fig. 6). However, when looking at the bottom two rows of Fig. 8, the CONTROL run of the model correctly simulates the positive correlations with the low-passed inverted NPO SP and SLPa Hawaii (Fig. 8c and d). Spatial correlations between Fig. 8c (Fig. 8d) and the same region in Fig. 6c (Fig. 6d) is $r = 0.97$ ($r = 0.97$). The TROP runs also recover these positive correlations in the central tropical Pacific, particularly for the SLPa Hawaii correlation map (Fig. 8h). Although the correlation coefficients in Fig. 8g and h are modest, these are mean correlation coefficients over 45 ensemble members, making even modest correlation values

(i.e., $|r| > 0.15$) significant at the $p < 0.05$ level. More importantly, the pattern correlation between the CONTROL and TROP ENSMEAN patterns is exceptionally high ($r = 0.93$ between Fig. 8c and g and $r = 0.99$ between Fig. 8d and h). Indeed, these results indicate that tropical Pacific SSTa directly drive a significant portion of the low-frequency variability in the subtropical node of the NPO.

6 Potential mechanism linking CPW variability to extratropical North Pacific Atmospheric variability

The results thus far have shown significant connections between variability in Hawaiian SLP and the CPW phenomenon, both at contemporary and quasi-decadal timescales. Figure 9 presents a potential mechanism explaining the dynamical link between the two. The 200 hPa streamfunction anomaly (Ψ') regression pattern associated with the CPW index (Fig. 9a; shading) shows a Rossby wavetrain originating in the central tropical Pacific and oriented north/south, with maximum amplitude centers in the Northern Hemisphere just to the south/southeast and north/
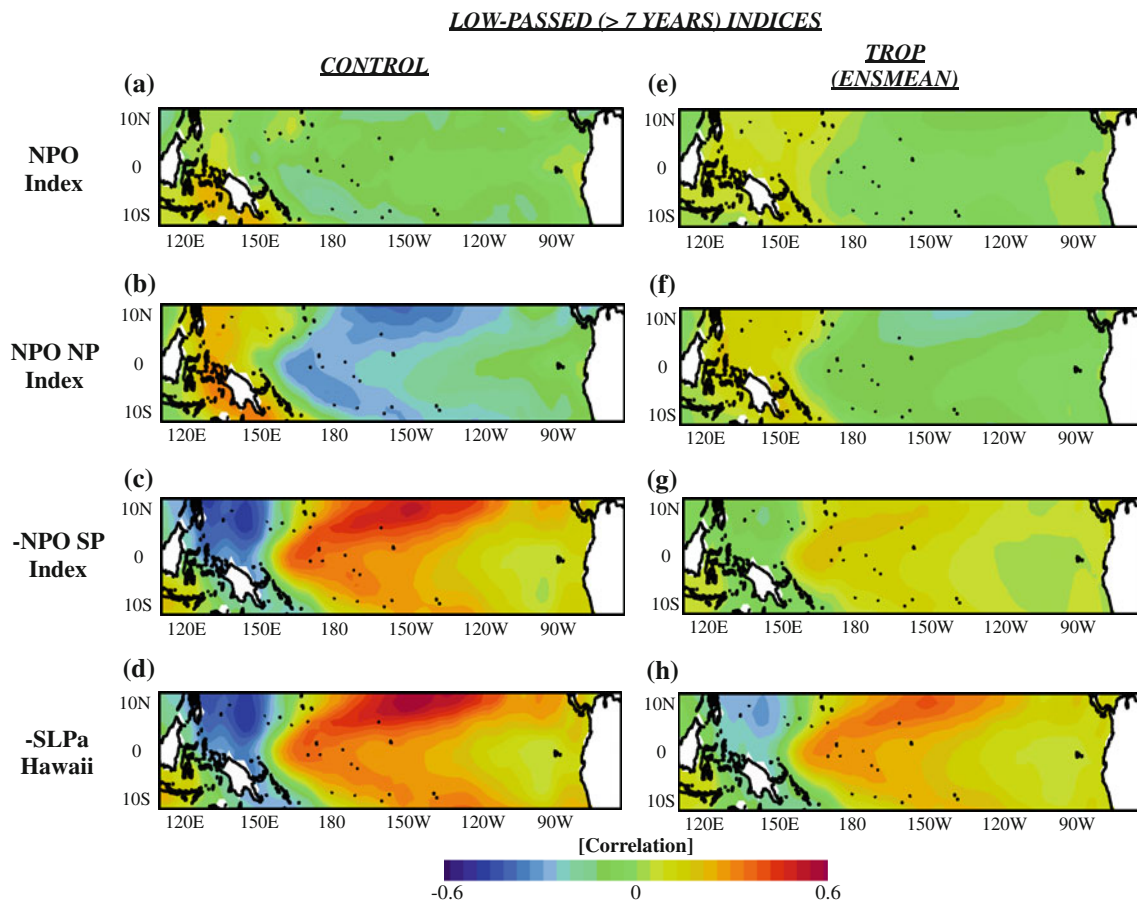
LOW-PASSED (> 7 YEARS) INDICES

Fig. 8 Correlation of NDJFM SSTa with the standardized low-passed NPO indices from the CONTROL run: **a** NPO index; **b** NPO NP index; **c** NPO SP index (*inverted*); **d** SLPa Hawaii index (*inverted*). **e–h** As in **a–d** but for the ensemble-mean correlation patterns from the TROP runs. For the ensemble-mean plots, correlation values $|r| \approx 0.15$ are considered significant at the $p < 0.05$ level

northwest of the Hawaiian Islands. This wavetrain projects directly onto the signature of the SLPa Hawaii index in the upper troposphere (Fig. 9a; line contours). To contrast the CPW-induced wavetrain with that of canonical ENSO, Fig. 9b shows the regression of 200 hPa Ψ' with the CanENSO index (shading) and the SLPa Hawaii index (contours). The wavetrain excited by variations in eastern tropical Pacific SSTa variability is displaced slightly east of that associated with the CPW and is oriented more north-eastward, projecting much less on the upper tropospheric Hawaiian SLPa signature (Fig. 9b, line contours) and more on the mean position of the AL (i.e., the region of strong negative Ψ' south of Alaska). In fact, across the far northern Pacific and into Alaska, note that negative streamfunction anomalies associated with eastern Pacific warmings project onto *positive* streamfunction anomalies associated with the SLPa Hawaii index.

Thus, there is a noticeable difference in the projection of the CPW phenomenon versus the canonical ENSO signature in the North Pacific, the former of which has a direct impact on the region near the Hawaii/NPO SP. The impact of these differences in teleconnection patterns will likely be important for seasonal and even decadal-scale predictions, and the differences warrant future studies.

7 Discussion and conclusions

The analyses presented in this paper support two key hypotheses involving the NPO: (1) While the NPO itself is stochastic, its individual nodes exhibit different behavior spatially and temporally; and (2) NPO SP variability at low frequencies is related to and forced in part by tropical Pacific SSTa variability. With its unique ties to CPW-type variability, which also contains quasi-decadal variability, the NPO SP may be an important contributor to tying together other large-scale modes of Pacific interannual and decadal climate variability.

The dissection of the NPO into its two poles reveals that the phenomenon is dominated by two different processes for each pole. By nature of being an oscillation, the NPO NP and NPO SP are correlated, especially at high frequencies.
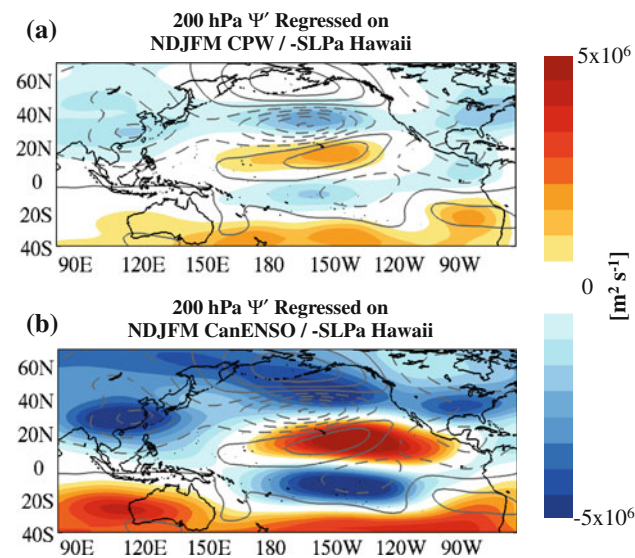
(a)

200 hPa Ψ′ Regressed on
NDJFM CPW / -SLPa Hawaii

(b)

200 hPa Ψ′ Regressed on
NDJFM CanENSO / -SLPa Hawaii

Fig. 9 **a** (*Shading*) Regression of Ψ′ (m^2s^{-1}) onto NDJFM values of the standardized CPW index. (*Contours*) Regression of Ψ′ (m^2s^{-1}) onto NDJFM values of the standardized inverted SLPa Hawaii index. **b** As in **a** but *shading* represents regression of Ψ′ (m^2s^{-1}) onto NDJFM values of the standardized CanENSO index. Positive (negative) regression coefficients are *solid* (*dashed*) for *line contours*

Indeed, the power spectra for all NPO indices are nearly identical for periodicities <2 years (Fig. 5a). But, the NPO NP power spectrum has no significant power at longer periods. The NPO SP power spectrum, by contrast, illustrates both high-frequency variability influenced by extra-tropical atmospheric circulation (Caballero and Anderson 2009) and significantly longer-term periodicity (4–10 years). The low-frequency nature of the NPO SP is best captured by the SLPa Hawaii index, which represents spatially the structure of the low-passed NPO index (Fig. 4c). A Hawaiian station record also verifies this low-frequency nature (Fig. 5b). The difference in the characteristics of each node illustrates the definition of the NPO (either EOF-based or a measure of dipole strength as done in this study) masks the importance of the NPO SP in its role in long-term North Pacific and tropical Pacific climate variability. Moreover, Table 1 reveals that, in observations, the NPO and NPO NP are nearly identical, indicating that the traditional definition of the NPO reflects mostly high-latitude SLPa variability. The weaker (though still significant) correlations between the NPO NP and NPO SP indices illustrate that, although 35% of the variance in one is related to variations in the other, 65% is due to other factors. This result, along with the power spectra results, suggest that one should carefully consider independently the two centers of action of the NPO, as they are mostly governed by different dynamics. The NPO NP is more intrinsic and is driven mainly by atmospheric "noise", thus producing a white-ish power spectrum. By contrast, the NPO SP still retains

important seasonal characteristics, likely linked to the "seasonal footprinting"/ENSO precursor signature. However, this node also derives a part of its low-frequency variability from forcing associated with tropical Pacific SSTa. Indeed, when the NPO index is low-passed and correlated with SLPa, the NPO NP node weakens substantially, while the NPO SP node remains prominent but shifted in location toward the east (Fig. 4c), into the region of the SLPa Hawaii index.

The relations between NPO SP variability and forcing from tropical Pacific SSTa was explored in observations and a simple model experiment. The power spectra of the TROP runs support hypothesis (2) above: the low-frequency characteristic of the NPO SP/SLPa Hawaii indices is still recovered in the tropically-forced only runs. When examining the SSTa correlation maps with the low-passed ICTP model indices, the patterns for the low-passed NPO SP and SLPa Hawaii in the CONTROL and TROP runs match well with the observations (Fig. 8). That is, the low-frequency nature of the NPO SP indeed projects strongly onto the central tropical Pacific SSTa field, in a pattern like that of the CPW phenomenon. Note, however, that the model erroneously captures weak (and negative) correlations between the low-passed NPO and NPO NP indices and tropical Pacific SSTs for both runs. This implies that, for the TROP run in particular, the tropical Pacific SSTa forcing projects primarily onto the subtropical North Pacific only at low frequencies. The negative correlation values may also reflect differences in remote and/or local influences on high-latitude SLP variations in the model versus observations.

Taken together with the results of Vimont et al. (2003), Anderson (2007a), and Di Lorenzo et al. (2010), the conclusions reached in this study offer a new link between the CPW, the NPO, and the NPGO at both seasonal and decadal timescales, akin to the ENSO-AL-PDO framework used to describe Pacific decadal climate variability. With the increase in variance of the CPW (Yeh et al. 2009) and the NPGO (Di Lorenzo et al. 2008) in recent decades, this CPW-NPO-NPGO links may become increasingly important in driving changes in the Pacific atmospheric, oceanic, and biological systems. This new link also offers a new perspective on ocean-atmosphere interactions in Pacific decadal climate studies. Traditionally, decadal-scale variability in extratropical Pacific SSTs are considered to be tied to integration of high-frequency atmospheric forcing into the ocean. Our results suggest there may be a feedback at work whereby low-frequency forcing *from* the ocean partially drives low-frequency variability in the North Pacific subtropical atmosphere. Still unknown, however, is the mechanism of the generation of the decadal-scale tropical Pacific SSTa. These anomalies may be generated locally or may be excited by variability and subduction of

subtropical Pacific SSTa. Such analyses would involve more complicated (and coupled) models than employed in this study.

Moreover, other SST areas may also play an important role in driving a fraction of low-frequency NPO SP variability. For example, Fig. 4d and all panels in Fig. 6 show significant anti-correlations between the low-passed NPO indices and SSTs in the western North Pacific. This region is also prominent in the characteristic NPGO SSTa pattern (cf. Fig. 4b of Di Lorenzo et al. (2008), with opposite sign). How this region impacts the NPO (or vice versa) remains a topic for future research.

More research on the CPW-NPO-NPGO links at both seasonal and decadal scales is needed. One missing component is an "atmospheric bridge" and/or "oceanic tunnel"-type mechanism which links these three secondary modes of variability together dynamically. Figure 9 offered initial evidence of a unique atmospheric bridge for the CPW phenomenon, with implications for changes in atmospheric circulation in North America and the Atlantic that are different than that associated with canonical ENSO. The differences, for example in the northeastern United States, between the CPW- and canonical ENSO-associated atmospheric circulation play a role in both seasonal forecasts and projections for long-term climate change. Parallel analyses like those reviewed and conducted in Alexander et al. (2002) are needed to further develop this hypothesized mechanism for the CPW and expand on its role in extratropical wintertime variability in the Northern Hemisphere. The analyses may also be expanded to explore the source of tropical Pacific SST variability.

Furthermore, our analysis of the low-frequency connections between the NPO and CPW were conducted with a fairly simple AGCM. Future studies should examine the connections between low-frequency changes in the NPO SP and both the tropical and extratropical signature in SSTs and also of the atmosphere as well. Such model runs would be integral for the "atmospheric-bridge"-type research route proposed above.

References

Alexander MA, Bladé I, Newman M, Lanzante JR, Lau NC, Scott JD (2002) The atmospheric bridge: the influence of ENSO teleconnections on air-sea interaction over the global oceans. J Climate 15:2205–2231

Anderson BT (2003) Tropical Pacific sea-surface temperatures and preceding sea level pressure anomalies in the subtropical North Pacific. J Geophys Res 108:4732. doi:10.1029/2003JD003805

Anderson BT (2004) Investigation of a large-scale mode of ocean-atmosphere variability and its relation to tropical Pacific sea surface temperature anomalies. J Climate 17:4089–4098

Anderson BT (2007) Intraseasonal atmospheric variability in the extratropics and its relation to the onset of tropical Pacific sea surface temperature anomalies. J Climate 20:926–936

Anderson BT (2007) On the joint role of subtropical atmospheric variability and equatorial subsurface heat content anomalies in initiating the onset of ENSO events. J Climate 20:1593–1599

Anderson BT, Maloney E (2006) Interannual tropical Pacific sea surface temperatures and their relation to preceding sea level pressures in the NCAR CCSM2. J Climate 19:998–1012

Ashok K, Behara SK, Rao SA, Weng HY, Yamagata T (2007) El Niño Modoki and its possible teleconnection. J Geophys Res 112:C11007. doi:10.1029/2006JC003798

Barsugli JJ, Battisti DS (1998) The basic effects of atmosphere-ocean thermal coupling on midlatitude variability. J Atmos Sci 55: 477–493

Bladé I (1997) The influence of midlatitude coupling on the low frequency variability of a GCM. Part I: no tropical SST forcing. J Climate 10:2087–2106

Bracco A, Kucharski F, Molteni F, Hazeleger W, Severijns C (2006) A recipe for simulating the interannual variability of the Asian summer monsoon and its relation with ENSO. Climate Dyn 28:441–460

Bretherton CS, Widmann M, Dymnikov VP, Wallace JM, Bladé I (1999) The effective number of spatial degrees of freedom of a time-varying field. J Climate 12:1990–2009

Caballero R, Anderson BT (2009) Impact of midlatitude stationary waves on regional Hadley cells and ENSO. Geophys Res Lett L17704. doi:10.1029/2009GL039668

Di Lorenzo E, Schneider N, Cobb KM, Chhak K, Franks PJS, Miller AJ, McWilliams JC, Bograd SJ, Arango H, Curchister E, Powell TM, Rivere P (2008) North Pacific Gyre Oscillation links ocean climate and ecosystem change. Geophys Res Lett 35:L08607. doi:10.1029/2007GL032838

Di Lorenzo E, Cobb KM, Furtado JC, Schneider N, Anderson BT, Bracco A, Alexander MA, Vimont DJ (2010) Central Pacific El Niño and decadal climate change in the North Pacific. Nat Geosci 3:762–765

Goddard L, Graham NE (1997) El Niño in the 1990s. J Geophys Res 102:10,423–10,436

Kistler R, Collins W, Saha S, White G, Woollen J, Kalnay E, Chelliah M, Ebisuzaki W, Kanamitsu M, Kousky V, van den Dool H, Jenne R, Fiorino M (2001) The NCEP-NCAR 50-year reanalysis: monthly means CD-ROM and documentation. Bull Am Meteor Soc 82:247–267

Kucharski F, Molteni F, Yoo JH (2006) SST forcing of decadal Indian monsoon rainfall variability. Geophys Res Lett 33:L03709. doi:10.1029/2005GL025371

Kucharski F, Bracco A, Yoo JH, Molteni F (2007) Low-frequency variability of the Indian monsoon–ENSO relationship and the tropical Atlantic: the "weakening" of the 1980s and 1990s. J Climate 20:4255–4266

Linkin ME, Nigam S (2008) The North Pacific Oscillation-West Pacific teleconnection pattern: mature-phase structure and winter impacts. J Climate 21:1979–1997

Mantua NJ, Hare SR, Zhang Y, Wallace JM, Francis R (1997) A Pacific interdecadal climate oscillation with impacts on salmon production. Bull Amer Meteor Soc 78:1069–1079

Molteni F (2003) Atmospheric simulations using a GCM with simplified physical parameterization. I: model climatology and

variability in multi-decadal experiment. Climate Dyn 20:175–191

Newman M, Compo GP, Alexander MA (2003) ENSO-forced variability of the Pacific Decadal Oscillation. J Climate 16:3853–3857

Penland C, Sardeshmukh PD (1995) The optimal growth of tropical sea surface temperature anomalies. J Climate 8:1999–2024

Quayle RG (1989) The Wolbach Dataset for global climate monitoring—Philanthropy and climatology. Bull Amer Meteor Soc 70: 1570

Rayner NA, Parker DE, Horton EB, Folland CK, Alexander LV, Rowell DP, Kent EC, Kaplan A (2003) Global analyses of sea surface temperature, sea ice, and night marine air temperature since the late nineteenth century. J Geophys Res 108:4407. doi: 10.1029/2002JD002670

Rogers JC (1981) The North Pacific Oscillation. J Climatol 1:39–57

Smith TM, Reynolds RW, Peterson TC, Lawrimore J (2008) Improvements to NOAA's historical Merged Land–Ocean Surface Temperature Analysis (1880–2006). J Climate 21:2283–2296

Torrence C, Compo GP (1998) A practical guide to wavelet analysis. Bull Am Meteor Soc 79:61–78

van Loon H, Meehl GA, Millhiff RF (2003) The Southern Oscillation in the early 1990s. Geophys Res Lett 30:1478. doi:10.1029/2002GL016307

Vimont DJ, Battisti DS, Hirst AC (2001) Footprinting: A seasonal connection between the tropics and mid-latitudes. Geophys Res Lett 28:3923–3926

Vimont DJ, Wallace JM, Battisti DS (2003) The seasonal footprinting mechanism in the Pacific: implications for ENSO. J Climate 16:2668–2675

Walker GT, Bliss EW (1932) World weather V. Mem Roy Meteor Soc 4:53–84

Yeh SW, Kug JS, Dewitte B, Kwon MH, Kirtman BP, Jin FF (2009) El Niño in a changing climate. Nature 461:511–514